esa

ECOSPHERE

River-valley morphology, basin size, and flow-event magnitude interact to produce wide variation in flooding dynamics

MOLLY VAN APPLEDORN [1,†] MATTHEW E. BAKER, AND ANDREW J. MILLER

Department of Geography and Environmental Systems, University of Maryland Baltimore County, 1000 Hilltop Circle, Baltimore, Maryland 21250 USA

Citation: Van Appledorn, M., M. E. Baker, and A. J. Miller. 2019. River-valley morphology, basin size, and flow-event magnitude interact to produce wide variation in flooding dynamics. Ecosphere 10(1):e02546. 10.1002/ecs2.2546 [Correction: article updated on January 8, 2019, after initial online publication: The year of publication in the suggested citation for this article was changed from 2018 to 2019.]

Abstract. Inundation dynamics are a key driver of ecosystem form and function in river-valley bottoms. Inundation itself is an outcome of multi-scalar interactions and can vary strongly within and among river reaches. As a result, establishing to what degree and how inundation dynamics vary spatially both within and among river reaches can be challenging. The objective of this study was to understand how river-valley morphology, basin size, and flow-event magnitude interact to affect inundation dynamics in river-valley bottoms. We used 2D hydraulic models to simulate inundation in four river reaches from Maryland's Piedmont physiographic province, and qualitatively and quantitatively summarized within- and among-reach patterns of inundation extent, duration, depth, shear stress, and wetting frequencies. On average, reaches from confined valley settings experienced less extensive flooding, shorter durations and shallower depths, stronger gradients of maximum shear stress, and relatively infrequent wetting compared to reaches from unconfined settings. These patterns were generally consistent across flow-event magnitudes. Patterns of within-reach flooding across event magnitudes revealed complex interactions between hydrology and surface topography. We concluded that valley morphology had a greater impact on flooding patterns than basin size: Inundation patterns were more consistent across reaches of similar morphology than similar basin size, but absolute values of inundation characteristics varied between large and small basins. Our results showed that the manifestation of out-of-bank flows in valley floors can vary widely depending on geomorphic context, even within a single physiographic province, which suggests that hydrologic and hydraulic conditions experienced on the valley floor may not be well represented by existing hydrologic metrics derived from discharge data alone. We thus support the notion that 2D hydraulic models can be useful hydrometric tools for cross-scale investigations of floodplain ecosystems.

Key words: floodplain ecosystem; geomorphology; hydraulics; hydrology; inundation; morphology; physiography.

Received 17 March 2018; revised 30 October 2018; accepted 20 November 2018. Corresponding Editor: Julia A. Jones.

[1] Present address: U.S. Geological Survey, Upper Midwest Environmental Sciences Center, 2630 Fanta Reed Road, La Crosse, Wisconsin 54603 USA.

† **E-mail:** mvanappledorn@usgs.gov

INTRODUCTION

Inundation dynamics are believed to be the master variable driving the structure and function of floodplain ecosystems (Junk et al. 1989, Ward et al. 2002). Overbank flood events drive vertical, lateral, and longitudinal exchanges of material and energy (Ward 1998, Amoros and Bornette 2002), ultimately affecting patterns of edaphic conditions, sediment deposition and scour, vegetation dispersal and forest succession, and biogeochemical cycling through space and time (Frye

and Quinn 1979, Hupp and Bazemore 1993, Megonigal et al. 1997, Tabacchi et al. 1998, Olde Venterink et al. 2006, Noe and Hupp 2009, Kaase and Kupfer 2016). As a result of such interactions, floodplain ecosystems are characterized by pronounced spatial (Scown et al. 2015) and temporal heterogeneity (Nakamura et al. 2007), making them among the most biophysically diverse ecosystems and both a high conservation and a restoration priority (Gregory et al. 1991, Malanson 1993, Naiman and Decamps 1997, Tockner and Stanford 2002, Bernhardt et al. 2005).

Flooding itself is an outcome of multi-scalar interactions among climate, landscape physiography, river-valley morphology, and local channel hydraulics. At broad scales, catchment size, shape, and land cover patterns constrain the availability and routing of water (Black 1997) that interplay with finer-scale controls on valley-bottom attenuation in complex ways (Woltemade and Potter 1994, Turner-Gillespie et al. 2003, Baker and Wiley 2009). For example, high upstream transport efficiency can produce frequent flooding if a given river-valley reach (i.e., a segment expressing relatively uniform valley morphology) is incapable of efficiently propagating the flood wave, or energetically intense floods if reach slope or valley width promotes deeper flow depths. Limited upstream conveyance combined with a reduced capacity for transport through the local reach can result in prolonged flooding. Thus, inundation dynamics may vary widely among reaches with different river-valley morphologies and contributing areas, even if they are from the same basin (Baker and Wiley 2009).

Inundation dynamics can also vary strongly on valley bottoms within a single reach. Interactions and feedbacks between surface and subsurface hydrology, biological organisms, topographic variation, and relative positioning on the valley floor's surface can produce within-reach gradients of inundation frequency, duration, and intensity (Miller 1995, Mertes 1997, Sparks and Spink 1998, Hupp 2000, Corenblit et al. 2011). Combinations of flooding attributes are expected to vary across different geomorphic features such that floodplains, ridges, swales, scroll bars, backswamps, and terraces experience inundation at different frequencies, at different depths, and for a range of durations. Valley-bottom landforms have been used extensively in the ecological literature as surrogates for hydraulic and hydrologic attributes in an effort to explain shifts in vegetation composition within river-valley reaches (Johnson et al. 1976, Osterkamp and Hupp 1984, Hupp and Osterkamp 1985, Tabacchi et al. 1990, 1998, Gregory 1992, Naiman et al. 1993, Pautou and Arens 1994, Marston et al. 1995, Bravard et al. 1997, Davies-Colley 1997, Hughes 1997, Bendix and Hupp 2000, Nakamura and Shin 2001, Gurnell and Petts 2003). Floodplain classifications have offered a way to reconcile reach-scale heterogeneity with broader physical constraints by associating geomorphic features on the valley-bottom surface with river-valley settings (e.g., Nanson and Croke 1992, Brierley and Fryirs 2005, Lóczy et al. 2012). However, existing classifications, including those that are process-based, have not explicitly described how within-reach distributions of inundation frequency, duration, depth, and shear stress relate to broader constraints of valley morphology and basin size. Our ability to develop expectations about how local eco-geomorphic relationships within a local river valley may translate to other valleys—even within the same river system—thus remains a challenge in floodplain ecology (Vaughan et al. 2009).

Recent advances in computing power and the proliferation of high-resolution topographic datasets have driven a shift toward more quantitative descriptions of fluvial geomorphic processes (Viles 2016), transforming scientists' abilities to map and quantitatively describe patterns of floodplain inundation. Two-dimensional (2D) hydraulic models, in particular, show promise as hydrometric tools for applications in floodplain ecology because of their ability to model complex flows and dynamic wetting and drying processes, capability of producing spatially continuous measures of floodplain inundation, and appropriateness in a wide range of scales and physical settings (Horritt and Bates 2002, Jowett and Duncan 2012). For example, 2D hydrodynamic models have been used to quantify hydrologic connectivity patterns among forest patches for the purposes of environmental flow regulation (Kupfer et al. 2015, Meitzen and Kupfer 2015) and to reveal hydrologic and hydraulic drivers of floodplain sedimentation dynamics that would have been difficult to ascertain by other approaches (Kaase and Kupfer 2016).

The objective of this study was to characterize the range of flooding dynamics observed in four river reaches of contrasting river-valley morphology (relatively unconfined vs. confined river-valley

settings) and size (large vs. small contributing areas) to understand how reach-scale patterns of inundation may be influenced by interactions between reach morphology and basin size. In particular, we asked: (1) How do inundation attributes vary among and within river reaches? (2) What is the relative importance of river reach morphology and basin scale on within-reach distributions of inundation attributes? and (3) How do these relationships change, if at all, across a gradient of flow-event magnitudes? We focused on describing patterns of five inundation attributes believed to be important in the structure and function of floodplain ecosystems: inundation extent, duration, depth, frequency, and shear stress. We expected that the patterns of inundation attributes will differ across river-valley settings such that valleys of relatively unconfined settings will experience a greater proportion of surface area wetted, but have relatively uniform distributions of duration, depth, frequency, and shear stress. We expected smaller inundation extents and more variable distributions of other inundation attributes in relatively confined valley settings. We also hypothesized that these patterns would remain consistent across basin sizes, but that absolute values of inundation extent, duration, depth, frequency, and shear stress would be greater in large basins than in small basins, and also increase with increasing flow-event magnitude. Here, we used 2D hydrodynamic models to qualitatively and quantitatively describe ecologically relevant inundation patterns in response to a gradient of relatively small to large overbank flow events.

Methods

Physiographic setting and study reaches

We examined floodplain inundation dynamics from basins located in the Maryland Piedmont physiographic province of the Chesapeake Bay

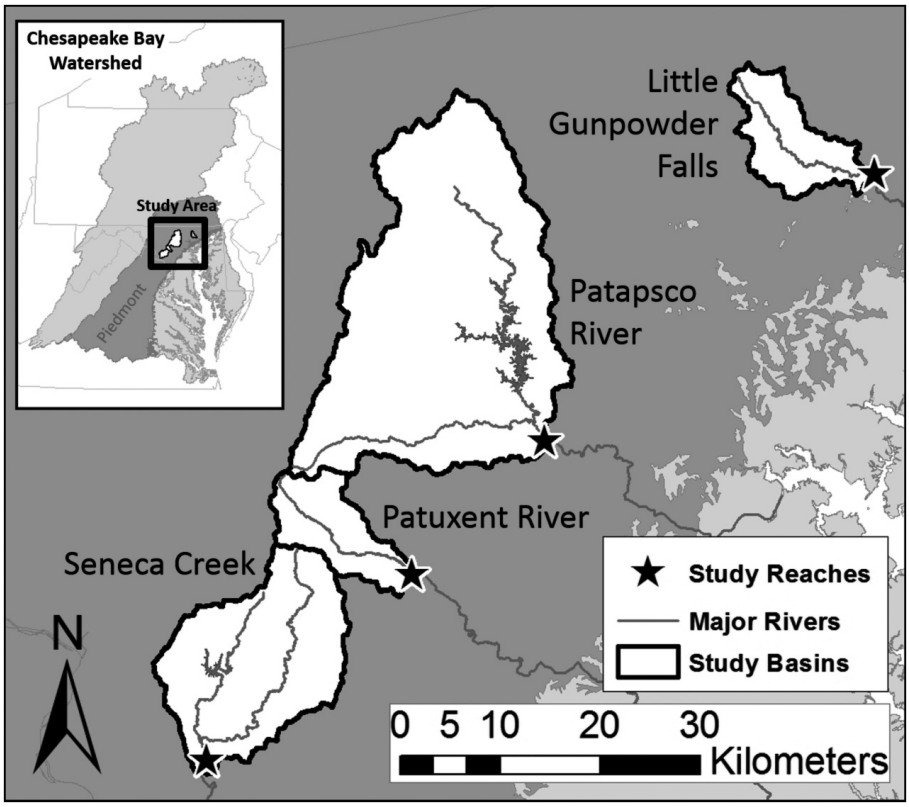

Fig. 1. The four study reaches are located in Maryland river basins from the Piedmont physiographic province of the Chesapeake Bay Watershed. Although climatically similar, the reaches differ in contributing area and river-valley morphology.

Watershed (Fig. 1). The Maryland Piedmont is characterized by rolling hills of moderate topography, typically 30–100 m in local relief, dissected by dendritic stream networks (White 2001). A variety of bedrock underlies the region including metamorphic rocks, shales, limestones, and sandstones. Legacy sediments from post-European settlement-era damming and agricultural land clearing are stored in floodplains and are believed to influence the functioning of contemporary bottomland ecosystems (Jacobson and Coleman 1986, Walter and Merritts 2008, Donovan et al. 2015). Piedmont stream channels are often incised, exposing a relatively thick layer of fine-grained settlement-era sediments overlying a Holocene organic-rich, hydric soil. Channel incision has resulted in contemporary "valley flats" that are believed to be at a greater elevation than associated with bankfull discharge (Leopold 1994). Valley flats have been interpreted as both floodplains (Wolman and Leopold 1957, Jacobson and Coleman 1986) and abandoned terraces (Walter and Merritts 2008, Merritts et al. 2011). Depositional bars, levees, backswamps, and terraces are landforms typically found in Maryland Piedmont river valleys. For the purposes of our analysis, we refer to the valley floor as all geomorphic features in valley-bottom settings that have the potential to be affected by inundation events, even if rarely, within the contemporary hydrologic regime.

We identified four U.S. Geological Survey (USGS) streamgages that spanned gradients of flood frequency and intensity observed in the Maryland Piedmont: Seneca Creek at Dawsonville (01645000), Patapsco River at Hollofield (01589000), Patuxent River at Unity (01591000), and Little Gunpowder Falls (01584500) (Appendix S1: Fig. S1). Valleys were scouted up and downstream of the streamgages to locate reaches that were (1) proximal to the streamgage, (2) comprised relatively undisturbed ecosystems, and (3) exhibited evidence of within-reach gradients of inundation dynamics. The resulting four reaches were located within the Piedmont, well above the boundary with the Coastal Plain physiographic province (Fig. 1). Reach lengths ranged from 0.4 km (Little Gunpowder Falls) to 3 km (Seneca Creek) (Table 1). The current valley floors of all four sites have aggraded to a level higher than the pre-settlement valley floor.

The reaches represent contrasting river-valley confinement, stream gradients, and basin scales (Table 1). Seneca Creek and the Patuxent River reaches had relatively wide river valleys compared to their respective channel widths, whereas the Patapsco River and Little Gunpowder Falls reaches had relatively constrained valley widths. Hereafter, we refer to Seneca Creek and the Patuxent River reaches as "unconfined" because virtually all of the river bank length is in contact with the alluvial plain. We refer to the Patapsco River and Little Gunpowder Falls reaches as "confined" because the river banks are in contact with the alluvial plain between 10% and 90% of their length. These definitions are similar to the terms "laterally unconfined channels" and "partly confined channels" Brierley and Fryirs (2005) and Rinaldi et al. (2013) used to describe river-valley settings. Stream gradients for the Patuxent River (2.2×10^{-3}) and Little Gunpowder Falls (2.3×10^{-3}) are approximately twice as steep as Seneca Creek (1.3×10^{-3}) and the Patapsco River (8.9×10^{-4}; Table 1). The contributing areas of the Seneca Creek (261 km^2) and Patapsco River (650 km^2) reaches are over twice as great as the contributing areas of either the Patuxent River (90 km^2) or Little Gunpowder Falls (93 km^2). Thus, our study design sought to maximize the potential to detect a range of inundation dynamics both within and among study reaches, with comparisons among the four reaches giving insight into the relative influence of river-valley morphology and basin scale on flooding patterns.

2D hydraulic model development

We used the U.S. Army Corps of Engineers' Hydrologic Engineering Center's River Analysis System two-dimensional hydraulic modeling software (HEC-RAS 2D, version 5.0.3, September 2016, U.S. Army Corps of Engineers, Hydrologic Engineering Center, Davis, California, USA) to characterize surface water inundation dynamics in each study reach. HEC-RAS 2D is a high-resolution numerical model that can perform hydrodynamic flow routing on an unstructured computational mesh. Developing a 2D hydraulic model for each study reach required four primary data inputs: a terrain model comprising terrestrial and bathymetric surfaces, flow resistance parameters, downstream boundary conditions, and inflow hydrographs. We developed a terrain model from high-resolution airborne LIDAR surveys collected between 2008

Table 1. Summary of physical attributes of study reaches and the associated streamgages used in this analysis.

Attribute	Seneca Creek	Patapsco River	Patuxent River	Little Gunpowder Falls
Streamgage name	Seneca Creek at Dawsonville	Patapsco River at Hollofield†	Patuxent River at Unity	Little Gunpowder Falls at Laurel Brook
USGS streamgage	01645000	01589000	01591000	01584500
Drainage area (km^2)	261	650	90	93
Study reach length (km)	3	1.6	2	0.4
Study reach area (km^2)	0.45	0.11	0.15	0.01
Channel width:valley width	Low	High	Low	High
Study reach position	Immediately downstream of streamgage	Near Woodstock, MD; 9 km upstream of Hollofield streamgage†	Immediately upstream of streamgage	Immediately upstream of streamgage
Upstream impoundments (year)‡	Clopper Lake (1975); Little Seneca Lake (1984)	Liberty Reservoir (1956)	None	None
Nearest documented historic milldam	8 km downstream	8 m downstream	At streamgage	At study reach
Dominant geology§	New Oxford Formation and Marburg Schist	Baltimore Gneiss	Wissahickon Formation	Lower Pelitic Schist
Percent forest¶	31.7	30.5	39.1	26.6
Percent impervious¶	14.3	7.2	2	5
Stream slope (ft/mile)¶	15.1	7.7	30.1	21.7
Study reach slope (%)#	0.131	0.089	0.22‖	0.23
Mean basin slope (%)¶	0.08	0.09	0.1	0.08
Flood frequency††, ‡‡	0.28	0.06	0.21	0.02
Flood intensity††, §§	1.59	1.95	1.14	1.1

† Hydrograph correction assessment in Van Appledorn (2016) and Van Appledorn et al. (*unpublished manuscript*) for hydrograph correction assessment.
‡ Years in parentheses are years of initial operation.
§ Maryland Geological Survey (1968).
¶ Thomas and Moglen (2010) and Ries et al. (2010).
# Slope calculated along thalweg of the river reach using the terrain models developed for HEC-RAS simulations.
‖ Slope upstream of road culvert = 0.25 and downstream of the culvert = 0.16.
†† Appendix S1.
‡‡ Flood frequency is the number of events per year of record.
§§ Flood intensity is calculated as median Q_{max}/Q_b, where Q_{max} = maximum discharge observed during an overbank event, Q_b = bankfull discharge.

and 2013 and channel cross sections in 2017; temporal changes in geomorphology (and hydrologic regime) were assumed to have negligible effect on model output at the scale of analysis. We assigned Manning's n value for river channels ($n = 0.03$) and floodplains ($n = 0.06$) following the recommendations of Chow (1959) and defined downstream boundary conditions by normal depth, estimated as the average slope of five down-channel elevation profiles extracted from the topo-bathymetric data using a geographic information system. Input hydrographs for model development and evaluation were derived from instantaneous discharge data of observed inundation events occurring in 2015 and 2016. We generated an unstructured computational mesh for each study reach that initially comprised a simple, uniform grid of 3.66 m × 3.66 m cell size and was subsequently modified to account for sharp changes in topography using breaklines. The resulting mesh comprised a range of cell configurations, though the majority of cells remained in uniform grids. The modeling framework employs a subgrid routine that allows for accurate representation of the underlying terrain even if mesh cell size is large. When compared to empirical measures of flooding attributes, model runs using these initial parameters, boundary conditions, input hydrographs, and meshes produced ecologically reasonable estimates of inundation extent, depth, and duration for the purposes of our study. Details of model development and evaluation may be found in Van Appledorn (2016).

Flood regime simulations

We used a series of five unsteady model simulations per study reach to characterize inundation regimes on the valley floors of the study reaches. The goal of the simulations was to understand the variability of inundation dynamics in response to a range of flood-event magnitudes represented in the hydrologic record. Each simulation was driven by a different input hydrograph derived from aggregated flood events identified in the instantaneous discharge record (Fig. 2). To develop the hydrographs, we first estimated bankfull discharge at each streamgage as the upper confidence interval of a 1.5-yr flow using PeakFQ (USGS 2007), a software package that implements the Bulletin 17B Flow Frequency Analysis (Interagency Advisory Committee on Water Data 1982). We qualitatively compared these estimates to the results of 2D hydraulic model simulations of observed inundation events occurring in 2015 and 2016 reported in Van Appledorn (2016) to assess whether the upper confidence interval of the 1.5-yr discharge was an appropriate estimate of bankfull discharge. Bankfull discharges were estimated from the simulation by stepping through the time series results to find when flows were not confined to the channel but overtopped the banks in at least two positions along the length of the river channel. We proceeded to use the PeakFQ estimate of bankfull discharge in subsequent analyses because it was never more than 8.21 cms (290 cfs) greater than the bankfull estimate derived from the 2D simulations for Patapsco River, Patuxent River, and Little Gunpowder Falls. At Seneca Creek, the upper confidence interval of the 1.5-yr flow (112.93 cms or 3988 cfs) overestimated bankfull discharge

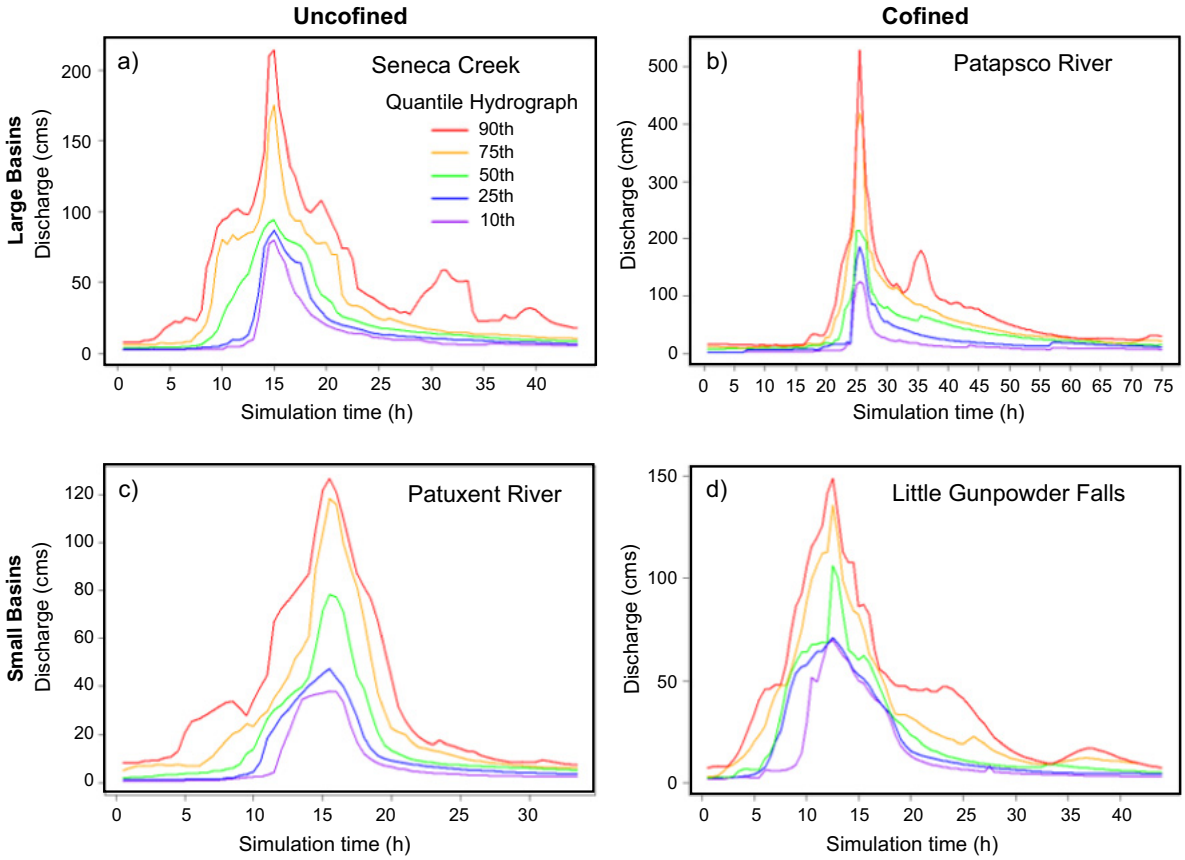

Fig. 2. Quantile hydrographs used in simulating inundation dynamics in four study reaches: Seneca Creek (a), Patapsco River (b), Patuxent River (c), and Little Gunpowder Falls (d). Five hydrographs were developed per study reach representing the 90th, 75th, 50th, 25th, and 10th quantiles of observed instantaneous discharges.

compared to 2D simulations; thus, we adjusted the estimate of bankfull discharge to 75.12 cms (2653 cfs) based on simulation results.

The bankfull discharge estimate was compared to the historical instantaneous discharge record at each streamgage to identify individual flood events, sequential discharges that met or exceeded the bankfull threshold. Flood events were extracted (including a period of 2 d prior and 2 d following the sequence of flows at bankfull or greater), and their peak discharges were temporally aligned, yielding an aggregate series of flood events for each study reach (Appendix S1: Table S1, Table S2, Fig. S2). We then computed the 10th, 25th, 50th, 75th, and 90th quantiles of instantaneous discharge at each 15-min time step across all flood events. These sequential discharges thus defined a series of five "quantile hydrographs" for each river reach. The quantile hydrographs are idealizations of historic flood hydrographs that reduce the idiosyncratic nuance of individual storm events in the hydrologic record, allowing for more general inferences of flooding behavior across study reaches. We subset the quantile hydrographs into 30-min time steps to serve as 2D model input. Coarsening the temporal resolution of the hydrographs did not produce numerical instability in the simulations and did not result in a loss of hydrologic variation or hydrograph integrity as the minimum and maximum discharge values and total event volumes were maintained. In order to characterize the magnitude of quantile hydrograph discharges in more familiar terms, we identified the recurrence interval of the maximum discharge observed in each quantile hydrograph by referencing the results of the PeakFQ analysis (Appendix S1: Table S3). Further details of quantile hydrograph development may be found in Appendix S1.

We ran five simulations per study reach, one simulation for each of the streamgage-specific quantile hydrographs. Models for Seneca Creek and the Patapsco River used the parameterization schema from validation events described in Van Appledorn (2016). We calibrated and parameterized models for the Patuxent River and Little Gunpowder Falls to approximate field observations of flooding extent and depth following inundation events in 2015 and 2016 and flooding descriptions from the NOAA NWS Flood Forecasting Center. Although no formal evaluation procedure was completed for these reaches, we expected that any differences in flooding dynamics between the two reaches due to contrasting river-valley morphology should be greater than any modeling errors due to uncertainty in model parameterization. We therefore included the results of the Patuxent River and Little Gunpowder Falls to make relative comparisons of flood regime among all four reaches. All simulations were run using a 10-sec computational time step; mapped output was generated at 5-min intervals.

Data analysis

The HEC-RAS modeling software produces both qualitative and quantitative results that may be used to characterize flooding dynamics within and across study reaches. First, we used the software's visualization tools to qualitatively describe the nature of dynamic inundation processes within and among reaches. We paid particular attention to spatial patterns of wetted extent, relative timing of inundation, and flow velocities because these attributes can be used to infer how surface topography, reach geomorphology, and hydrology interact to influence wetting and drying processes. We also examined dynamic mapped output to characterize temporal patterns of inundation. For each simulation, we calculated the time to peak wetted extent (TTP_{WE}) as the length of time from initial observations of out-of-channel flows to the time the maximum wetted extent was achieved, expressed as the proportion of the total duration out-of-channel flows. We also calculated the time to peak discharge (TTP_Q) for each input hydrograph as the length of time from initial bankfull discharge to peak discharge, expressed as a proportion of the total duration the hydrograph achieved or exceeded bankfull discharge. To match the temporal resolution of dynamic simulation output, we linearly interpolated between the 15-min time steps of the original quantile hydrographs to identify when bankfull discharge would occur at 5-min intervals.

Second, we quantified five ecologically relevant attributes of flooding within the valley margins of each study reach using model output: inundation extent, duration, depth, shear stress, and frequency. We defined the valley margins morphologically as the transition between the relatively flat, low elevation areas and the

relatively steep hillslopes (sensu Fryirs et al. 2016). Areas within the valley margins include the active (genetic) floodplain and other valley floor landforms such as terraces (Fryirs et al. 2016) and are expected to exhibit different environmental conditions (e.g., sediment characteristics, hydrology, soil depth) than hillslope areas because of their morphology and position within the landscape. We delineated valley margins by examining distributions of slope and curvature measures of LIDAR-derived elevations, with shifts in slope and curvature values distinguishing steep hillslopes from relatively flat valley floors; orthoimages were used as supplementary information to confirm the location of the valley margin. We expected our results would be robust to the delineations due to the magnitude of topographic relief observed between the valley bottom and hillslopes during site visits to the study reaches and geospatial analyses. We extracted the time series of modeled water depths for each computational mesh cell within the valley floor from the HEC-RAS simulations. To minimize the effects of any minor wetting remaining from the model spin-up process, we excluded depths <2.5 cm from the depth time series. We then identified and summed the area of cells experiencing submergence at any point during a simulation and calculated the proportion of valley floor inundated by dividing this value by the total valley floor area. We calculated inundation duration for each valley floor mesh cell as the total length of time a mesh cell was submerged. We reported patterns in inundation depth as the maximum water depth achieved over the length of a simulation; exploratory analyses revealed no substantive differences in our results when maximum depth was used to characterize submergence patterns compared to mean or median depth values. We also extracted estimates of maximum shear stress for valley floor mesh cells from each simulation. We summarized patterns of duration, depth, and shear stress within and among reaches using cumulative relative frequency distributions. Statistical summaries were completed using R statistical software (R Development Core Team, 2016).

We also mapped patterns of inundation frequency for every mesh cell using a method that allows for standardized comparisons within and among reaches. For every valley floor mesh cell, we identified the time of first inundation exceeding 2.5 cm in depth during the 90th quantile event simulation, and identified the discharge value occurring in the simulation at that time step from the input hydrograph. The discharge was then related to the results of the PeakFQ flow frequency analysis to extract the flow's annual exceedance probability, expressed as a percentage. Thus, exceedance probabilities were mapped for each valley floor mesh cell by referencing results from the hydrologic analysis of the annual maximum flood series. The resulting map was a spatially explicit depiction of the probability that the discharge necessary to inundate a particular mesh cell is equaled or exceeded in a given year. We used cumulative relative frequency distributions to summarize inundation frequencies across reaches.

Results

Qualitative flooding attributes

Reaches with similar morphologies exhibited qualitatively similar patterns of flooding dynamics despite differences in basin scales. Flood events at Seneca Creek (Videos S1–S5) and Patuxent River (Videos S11–S15) were characterized by extensive valley floor inundation, even during the 10th quantile hydrograph event in which maximum discharges corresponded to 1.3-yr and 1.8-yr events, respectively. Flooding at Seneca Creek initiated at the lower portion of the reach, on the left bank, where back-flooding quickly expanded over the internal portion of the floodplain surface in an up-valley direction (Fig. 3). Within the right bank, flow from the channel overtopped the banks and followed an internal drainage network in both up- and down-valley directions. Eventually, all flow was routed down-valley and the full extent of inundation was subsequently achieved. In the morphologically similar Patuxent River reach, patterns of valley-floor inundation also appeared to be a function of back-flooding, overbank flows, and internal drainage processes. These processes were influenced by the presence of a road embankment in the middle of the study reach that contributed to backwater effects and relatively longer durations of inundation upstream of the road crossing, whereas relatively high-velocity flows were observed immediately downstream of the culvert. These dynamic patterns were observed particularly

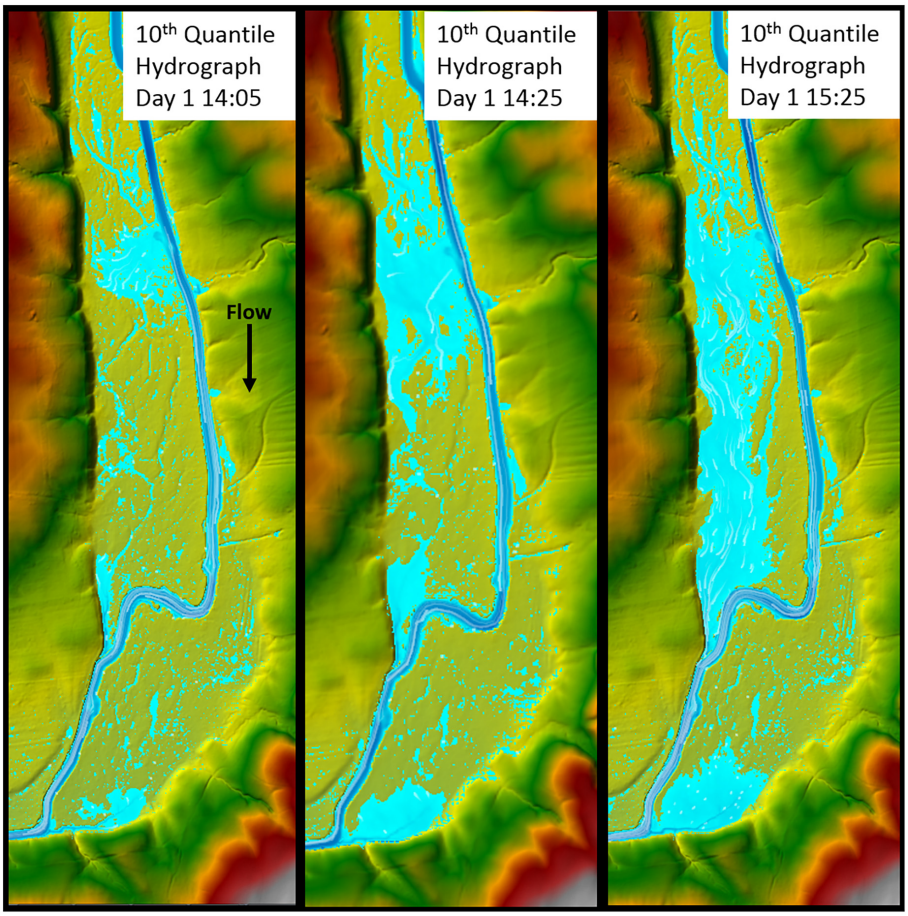

Fig. 3. Time series of model stills from 10th quantile hydrograph event as examples of distinctive flooding patterns in Seneca Creek. Darker blue indicates deeper water depths. White lines indicate velocity and direction of flow: Longer lines indicate faster velocities; blunter end indicates forward direction. Overbank inundation in the left bank floodplain is initially caused by back-flooding as the river valley narrows and channel turns sharply (bottom of left panel). Within 20 min, the right bank floodplain is rapidly inundated when overbank discharge proceeds down-valley through existing secondary channels and standing surface water and reconnects with channel mainstem; back-flooding on left bank floodplain still occurs, but velocity begins to slow likely due to upstream, right bank storage. Within approximately 1 additional hour, the maximum extent of inundation is achieved and the direction of flow on the right bank becomes entirely down-valley.

during simulations of the 10th and 25th quantile hydrographs.

Compared to the unconfined Seneca Creek or Patuxent River reaches, flooding was not as extensive and generally constrained to be near the channel for the Patapsco River (Videos S6–S10) and Little Gunpowder Falls (Videos S16–S20) reaches during any given quantile event. The confined reaches lacked any internal drainage networks, and flooding tended to occur along the banks, point bars, and topographic lows via direct fill. Back-flooding was not as prominent a process as it was at the Seneca Creek and Patuxent River reaches, though it did occur locally (Fig. 4).

Unconfined reaches took longer than their confined counterparts to achieve maximum wetted extent as a proportion of the total duration of out-of-channel flows (Table 2). Maximum extents were achieved around the total duration midpoint at Seneca Creek for the 50th quantile event and larger (TTP_{WE}: 0.42–0.46) and for all event

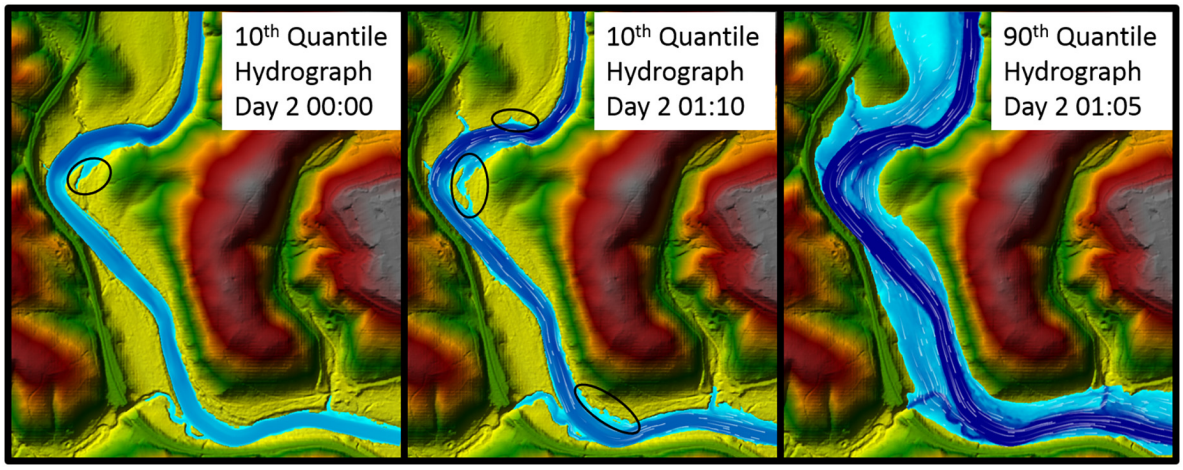

Fig. 4. Time series of model stills from 10th quantile hydrograph (left, middle) and 90th quantile hydrograph (right) models as examples of typical flooding patterns in Patapsco. Darker blue indicates deeper water depths. White lines indicate velocity and direction of flow: Longer lines indicate faster velocities; blunter end indicates forward direction. Early inundation occurs in topographically low depressions nearest to the channel (left panel, circled region). At the hydrograph maximum, the right bank floodplain experiences slight inundation due to back-flooding, but it is minimal in extent and very brief. During the flood peak (middle panel), the majority of the valley bottom remains dry with only minor wetting in other topographic lows (upper and lower circles) and a flow-through depression (middle circle). The majority of the floodplain is inundated at the hydrograph maximum for the 90th quantile event, and all flow is down-valley (right panel).

Table 2. Summary of observed time to peak discharge (TTP_Q) as derived from hydrologic inputs compared to time to peak wetted extent (TTP_{WE}) as derived from simulation results for study sites of contrasting valley confinement (U = unconfined, C = confined) and basin size (L = large, S = small).

	Quantile hydrograph				
Time to peak metric	10th	25th	50th	75th	90th
Seneca Creek (U, L)					
Hydrograph TTP_Q	0.81	0.55	0.39	0.5	0.48
Simulated TTP_{WE}	0.29	0.3	0.45	0.46	0.42
Patapsco River (C, L)					
Hydrograph TTP_Q	0.47	0.43	0.56	0.3	0.23
Simulated TTP_{WE}	0.31	0.14	0.13	0.15	0.15
Patuxent River (U, S)					
Hydrograph TTP_Q	0.65	0.62	0.52	0.52	0.52
Simulated TTP_{WE}	0.56	0.56	0.52	0.48	0.55
Little Gunpowder Falls (C, S)					
Hydrograph TTP_Q	0.39	0.59	0.5	0.48	0.51
Simulated TTP_{WE}	0.25	0.37	0.39	0.45	0.34

Notes: TTP_Q for hydrologic inputs is calculated as the length of time from initial bankfull discharge to peak discharge, expressed as a proportion of the total duration the hydrograph achieved or exceeded bankfull discharge. For simulation results, TTP_{WE} is calculated as the length of time from initial observations of out-of-channel flows to the time the maximum wetted extent is achieved, expressed as the proportion of the total duration out-of-channel flows were observed in dynamic modeling results.

magnitudes at the Patuxent River (TTP_{WE}: 0.48–0.56) (Table 2). Simulation TTP_{WE} values averaged to be within 76% and 94% of hydrograph TTP_Q values across all event magnitudes for Seneca Creek and the Patuxent River, respectively. At Seneca Creek, differences between simulation TTP and hydrograph TTP were greatest in low-magnitude events, indicating the potential

for storage effects of the valley bottom to be greater for low flows. In the confined reaches, lateral connectivity lasted longer during the recession period compared to hydrologic inputs: TTP_{WE} values of the simulations were within 46% and 72% of hydrograph TTP_Q values across all event magnitudes for the Patapsco River and Little Gunpowder Falls, respectively (Table 2). In these reaches, drainage of topographic lows and point bars near the channel was slow (Videos S6–S10; S16–S20), likely influencing the simulated TTP_{WE} values.

Inundation extent

Patterns of flooding extent were fundamentally different between reaches of contrasting morphologies: Unconfined reaches experienced consistently more extensive flooding for any given flood magnitude compared to confined reaches of similar scale. At least 47% of the valley floor surface was inundated during the 10th quantile simulation at Seneca Creek and Patuxent River reaches, but no >17% of the valley floor surface was inundated during similar events at either the Patapsco River or the Little Gunpowder Falls reaches (Table 3). Proportionally more of the Seneca Creek floodplain was inundated during the largest event magnitude compared to the Patapsco River floodplain (97% vs. 84%) despite the fact that the peak discharge observed during simulations represented a 4.8-yr flow at Seneca Creek and 10.8-yr flow at Patapsco River (Appendix S1: Table S3).

The relationship between inundation extent and flood magnitude appeared to be a function of basin scale. Reaches from larger basins experienced a step change in the proportion of valley floor inundated between the 50th and 75th quantile events. Inundated areas of the Seneca Creek and Patapsco River floodplains increased by nearly 45% and 90% between the 50th and 75th quantile flood events, respectively. In contrast, inundation extents increased by only 5% and 18% between the 50th and 75th quantile flood events for the Patuxent River and Little Gunpowder Falls reaches, respectively.

Table 3. The proportion of floodplain inundated during five simulated event magnitudes for study sites of contrasting valley confinement (U = unconfined, C = confined) and basin size (L = large, S = small).

Study site	Quantile hydrograph				
	10th	25th	50th	75th	90th
Seneca Creek (U, L)	0.55	0.62	0.72	0.95	0.97
Patapsco River (C, L)	0.14	0.27	0.43	0.79	0.9
Patuxent River (U, S)	0.6	0.7	0.79	0.83	0.84
Little Gunpowder Falls (C, S)	0.17	0.18	0.28	0.33	0.38

Inundation duration

Inundation duration was longer and more uniformly distributed throughout the valley floor surface in the unconfined Seneca Creek and Patuxent Rivers compared to their morphologically different counterparts (Fig. 5). Over 20% of the Seneca Creek valley floor surface was inundated for the entire duration of each simulated event (Fig. 5b; Appendix S1: Fig. S3), and median durations were at least three times greater than those of the Patapsco River (Fig. 5a). Steep increases in the cumulative relative frequency distribution at short durations for the Patapsco River valley floor followed by gradual increases indicate that a relatively small proportion of the floor was briefly inundated, and an even smaller proportion inundated for periods longer than 50 h, with very little area submerged for 15–50 h (Fig. 5b). Median flood durations were also generally longer for the Patuxent River reach than for the Little Gunpowder Falls reach, the latter which experienced median durations of 0 h due to relatively large proportions of the valley floor never becoming wetted (Fig. 5c). The range of duration values was more limited in valley floors from unconfined river-valley settings compared to confined reaches, a pattern that was consistent when considering the entire valley floor or only areas wetted during an event (Appendix S1: Fig. S4, Table S4). In addition, the interquartile range of durations for only wetted cells ranged from 1.4 to 2.4 times greater for Little Gunpowder Falls than for the Patuxent River for any given simulation; the interquartile ranges for wetted areas of the Patapsco River were greater than those of Seneca Creek for the 10th–50th quantile events.

Inundation lasted longer at reaches with greater contributing areas than for those in smaller basins (Fig. 5). Median durations were up to 3.9 h longer at the Patapsco River compared to the Little Gunpowder Falls valley floor across all quantile events. The Patapsco River and Little

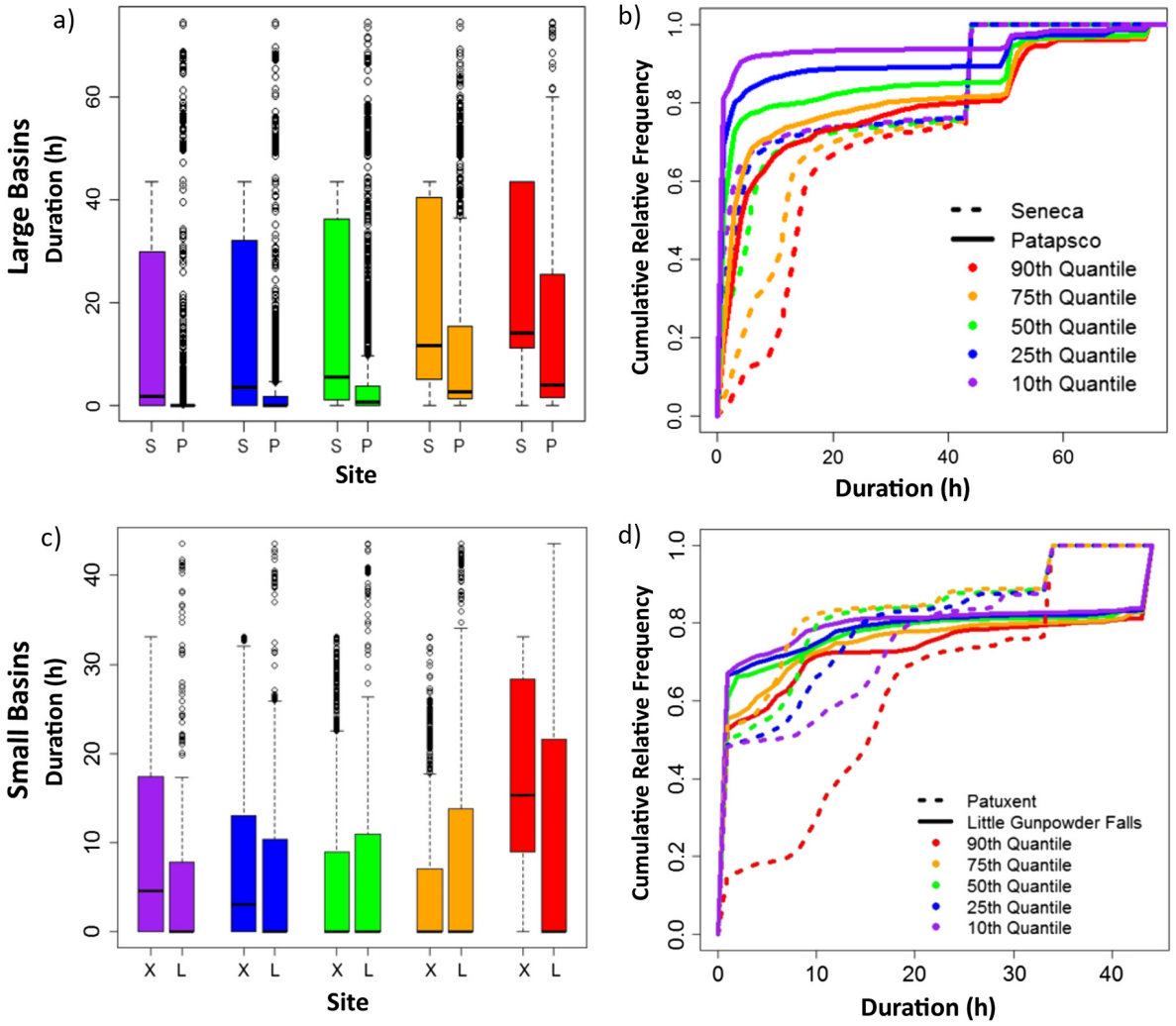

Fig. 5. Inundation duration on the valley floor surface by quantile hydrograph event for large basins (Seneca Creek = S, Patapsco River = P; panels a and b) and smaller basins (Patuxent River = X, Little Gunpowder Falls = L; panels c and d) expressed as absolute values (a, c) and cumulative relative frequency distributions (b, d). Horizontal lines in a and c indicate median values; points falling outside the whiskers are >1.5 times the interquartile range. Distributions are for both unwetted and wetted areas of the valley floors; for distributions summarizing only wetted areas, see Appendix S1.

Gunpowder Falls reaches had median durations of 0 h during smaller magnitude events, however, because large proportions of the valley floor did not experience any wetting (Table 3). Median duration was up to 12 h longer at Seneca Creek than at the Patuxent River for the 25th, 50th, and 75th quantile events. In the 10th and 90th quantile events, the median duration at the Patuxent River was greater than that at Seneca Creek (though never by more than 3 h).

Maximum event depth

Unconfined reaches experienced greater inundation depths than in confined reaches for most events (Fig. 6). Median values of maximum depth achieved during the 10th–50th quantile events ranged from 0.01 to 0.12 m over the entire Seneca Creek valley floor, while median depths were zero for the same magnitude events at the Patapsco River. During larger events, the Patapsco River valley floor experienced greater depths

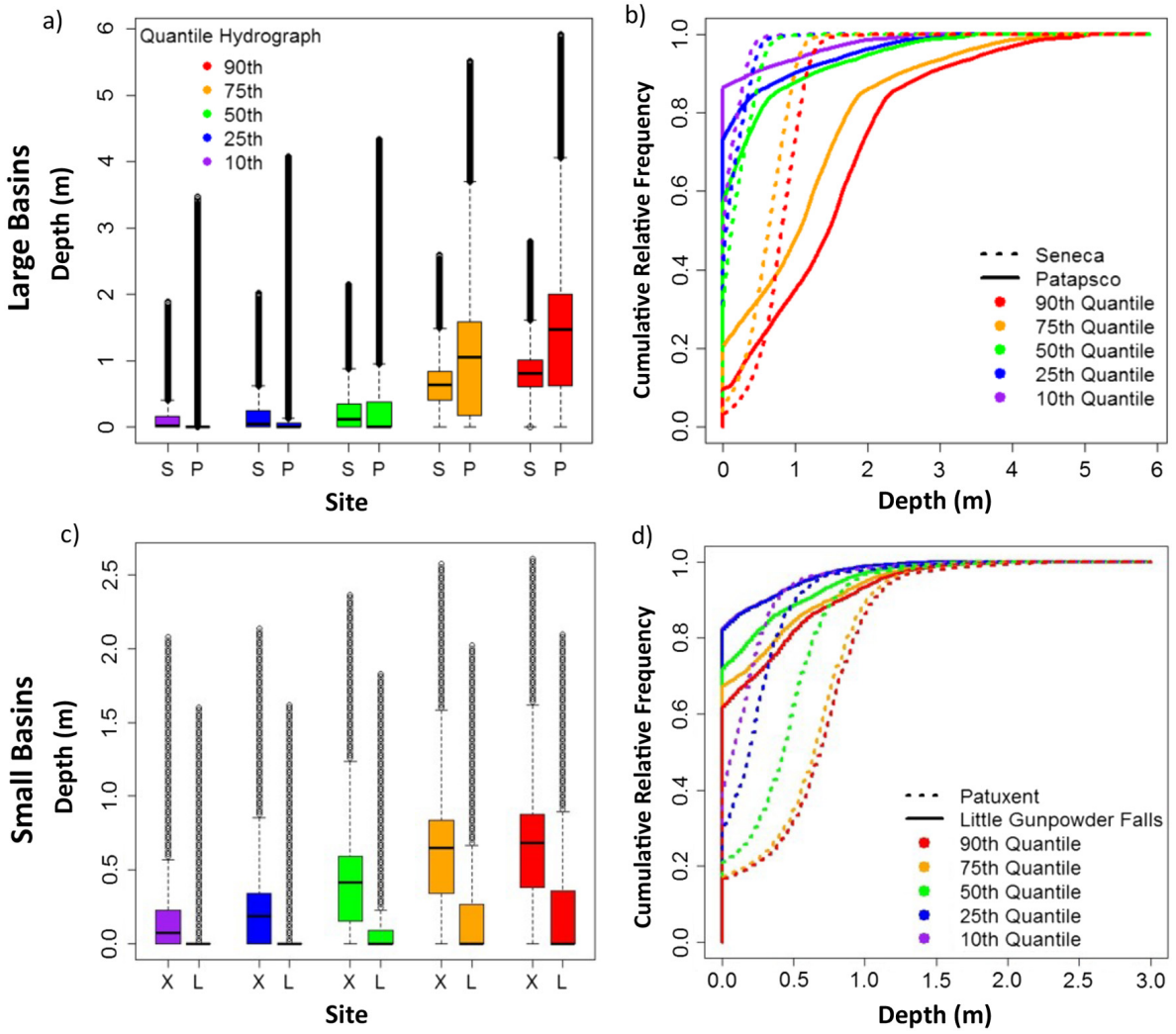

Fig. 6. Maximum inundation depth on the valley floor surface by quantile hydrograph event for large basins (Seneca Creek = S, Patapsco River = P; panels a and b) and small basins (Patuxent River = X, Little Gunpowder Falls = L; panels c and d) expressed as absolute values (a, c) and cumulative relative frequency distributions (b, d). Horizontal lines in (a) and (c) indicate median values; points falling outside the whiskers are >1.5 times the interquartile range. Distributions include wetted and unwetted valley floor areas; for distributions summarizing only wetted areas, see Appendix S1.

(median values of 1.06–1.46 m) than Seneca Creek (median values of 0.63–0.81 m). Median values of maximum event depths were greater in the Patuxent River valley floor (0.07–0.69 m) compared to the Little Gunpowder Falls (0 m) across all five events, but were likely influenced by the road embankment along the Patuxent River (Videos S11–S15).

Reaches with greater contributing areas experienced shifts in the distribution of inundation depths between the 50th and 75th quantile events that were not evident in reaches from smaller basins (Fig. 6). Sequential increases in median and maximum values were greatest between the 50th and 75th quantile events for Seneca Creek and Patapsco River floodplains. For example, the median depth of the 75th quantile event at Seneca Creek was over five times larger than that of the 50th quantile event (0.12 m vs. 0.63 m), and median depth increased from

0 m to 1.06 m at the Patapsco River for the same interval (Appendix S1: Table S6). In contrast, reaches from smaller basins did not exhibit peak changes in the median and maximum depths between the 50th and 75th quantile events. Rather, increases in distribution medians and maxima with increasing event magnitude remained modest compared to shifts observed in reaches from larger basins (Appendix S1: Table S5).

Maximum shear stress

Confined reaches experienced greater variability in maximum event shear stress than their unconfined counterparts across all event magnitudes and averaged greater maximum shear stress for most event magnitudes (Tables 4 and 5 and Fig. 7). Standard deviations of maximum event shear stress were at least 3.5 times as great in Patapsco River reach compared to Seneca Creek when comparing the entire valley floor surface

Table 4. Median and standard deviation of event maximum shear stress (N/m^2) across five simulated event magnitudes for study sites of contrasting valley confinement (U = unconfined, C = confined) and basin size (L = large, S = small).

	Quantile hydrograph				
Summary statistic	10th	25th	50th	75th	90th
Seneca Creek (U, L)					
Median	1.44	1.82	2.25	8.04	9.96
SD	2.83	2.94	3.25	4.75	5.31
Patapsco River (C, L)					
Median	8	8.71	6.85	18.39	23.94
SD	11.91	13.02	14.76	16.65	19.11
Patuxent River (U, S)					
Median	3.8	6.03	11.11	15.37	16.09
SD	10.26	10.17	10.37	10.59	10.73
Little Gunpowder Falls (C, S)					
Median	0	0	0	0	0
SD	7.9	7.98	9.11	10.07	10.6

Note: Values summarize shear stress across all valley floor mesh cells, including those remaining dry throughout the duration of the simulation.

Table 5. Median and standard deviation of event maximum shear stress (N/m^2) across five simulated event magnitudes for study sites of contrasting valley confinement (U = unconfined, C = confined) and basin size (L = large, S = small).

	Quantile hydrograph				
Summary statistic	10th	25th	50th	75th	90th
Seneca Creek (U, L)					
Median	1.77	2.11	2.44	8.04	9.96
SD	2.88	2.99	3.26	4.74	5.31
Patapsco River (C, L)					
Median	8.14	9	7.04	18.67	24.04
SD	11.92	13.03	14.81	16.56	19.07
Patuxent River (U, S)					
Median	3.88	6.08	11.11	15.37	16.14
SD	10.33	10.2	10.35	10.56	10.71
Little Gunpowder Falls (C, S)					
Median	8.24	8.47	7.28	8.24	8.62
SD	15.29	15.22	14.19	14.39	14.73

Note: Values summarize shear stress across only mesh cells experiencing inundation during a given event.

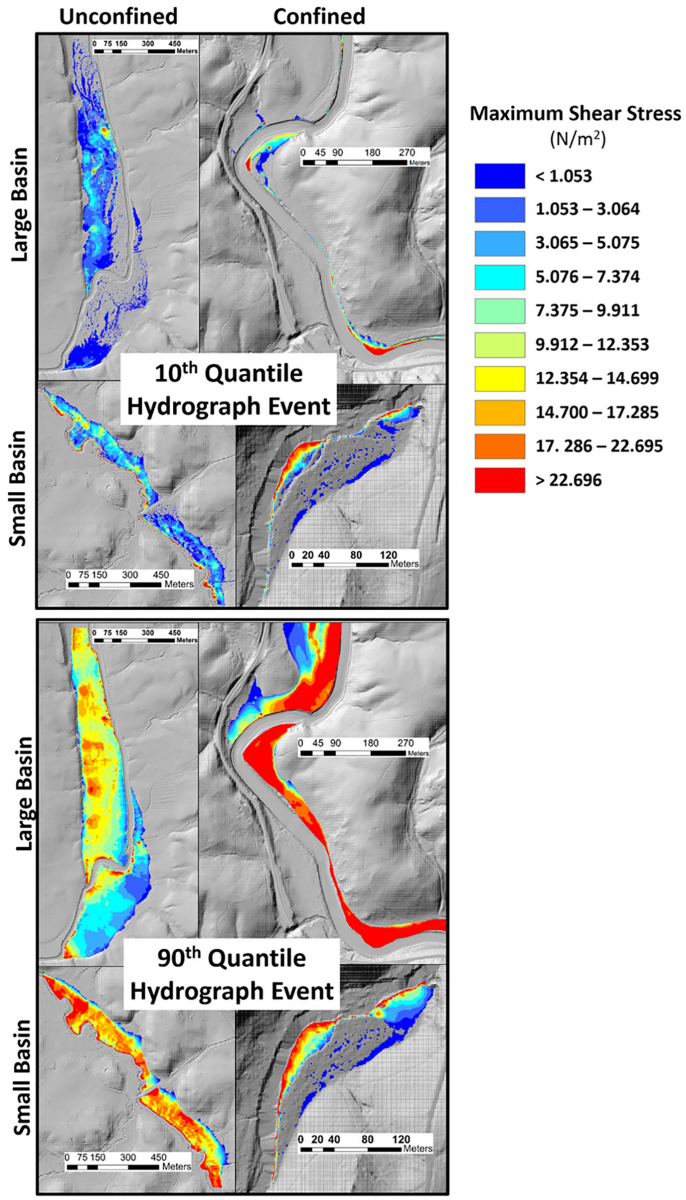

Fig. 7. Spatial distributions of shear stress modeled during a low-magnitude flood event (10th quantile hydrograph event) and a high-magnitude flood event (90th quantile hydrograph event).

and only the wetted portions. In wetted portions of the valley floor, the median floor shear stress was always at least twice as great in Patapsco River compared to Seneca Creek, even approaching five times greater in Patapsco River (8.14 N/m^2) compared to Seneca Creek (1.77 N/m^2) during low-magnitude events (10th and 25th quantile hydrograph simulations). The wetted portions of the confined Little Gunpowder Falls valley floor had median shear stress values over twice as great as the unconfined Patuxent River during low-magnitude events, but the Patuxent River valley floor experienced greater shears than Little Gunpowder Falls in simulations using the 50th–90th quantile hydrographs (Table 5).

The two large reaches both experienced a noticeable shift in the distribution of event maximum shear stresses from the 50th to 75th

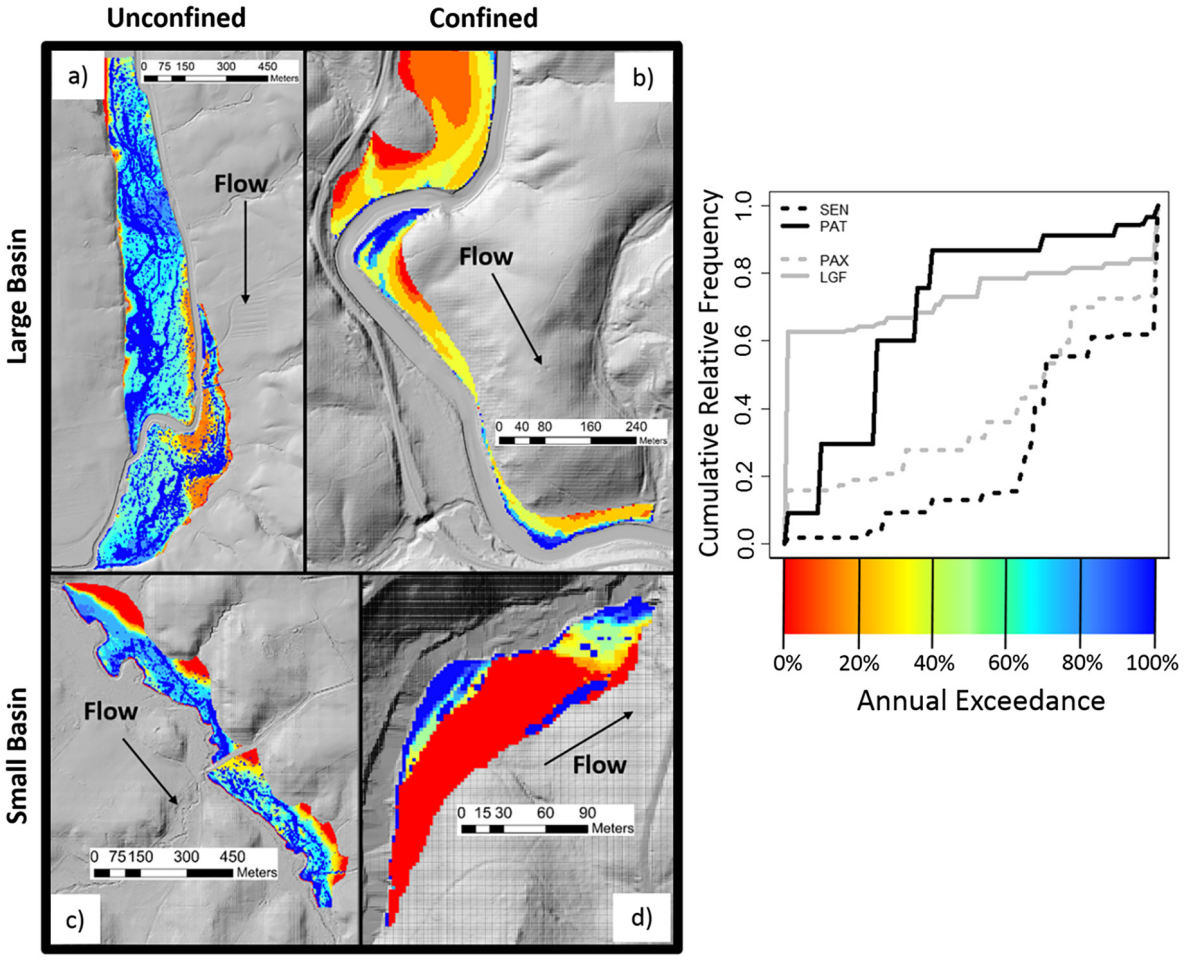

Fig. 8. Spatial distributions of annual exceedance values for the four study reaches (a = Seneca Creek, b = Patapsco River, c = Patuxent River, and d = Little Gunpowder Falls) and their cumulative relative frequency distributions of annual exceedance values (SEN = Seneca Creek, PAT = Patapsco River, PAX = Patuxent River, and LGF = Little Gunpowder Falls). Blue locations are more likely to be wetted in any given year; red locations are where inundation is rare. Note that areas with exceedance values equal to zero (red) may become inundated during events larger than those simulated in this analysis.

quantile events that was not apparent in the smaller reaches. Median values ranged from 2.65 to 3.58 times greater during the 75th quantile event compared to the 50th quantile event in both large reaches, with the greater shifts apparent in Seneca Creek, while other increases in median values across event magnitudes were always less than a factor of 1.3 (Tables 4 and 5; Appendix S1: Fig. S5). No such shifts were observed for the two smaller reaches, where median shear stresses remained steady (Little Gunpowder Falls) or experienced relatively steady increases with increasing event magnitudes (Patuxent River).

Inundation frequency

Valley floors in unconfined river-valley reaches had greater proportions of their areas likely to become inundated in any given year than valley floors in confined river-valley reaches (Fig. 8; Appendix S1: Fig. S6). Half of the Seneca Creek valley floor area was expected to be inundated during flows recurring at least every 1.2 yr (1.4 yr for the Patuxent River). In contrast, flows

recurring approximately every 6 yr were necessary to inundate half of the Patapsco River valley floor. Even under the largest simulated event magnitude, an event with an annual recurrence probability of 6.3 yr, less than half of the valley floor area of the Little Gunpowder Falls reach was wetted. Internal drainage networks in unconfined river-valley reaches tended to become wetted at very low discharges and were expected to carry flow annually, if not more often (Fig. 8a, c). Basin scale appeared to be less related to patterns of inundation frequency than the degree of valley confinement because no clear trends in inundation frequencies were noticeable across reaches of similar size.

Discussion

The importance of river-valley morphology

River-valley morphology had a greater impact on flooding patterns than basin size in our study reaches. This finding is consistent with the idea that the hydraulic geometry of a reach—both channel and valley-bottom morphology—directly affects the distribution of flow extent and depth for any given discharge (Leopold and Maddock 1953). As functions of streamflow regimes, inundation regimes result from complex, multi-scalar interactions among biophysical attributes (Woltemade 1994, Woltemade and Potter 1994, Baker and Wiley 2009, Fryirs and Brierley 2013) and anthropogenic impacts on hydrology via direct regulation (e.g., Karim et al. 2015, Stone et al. 2017), land use (e.g., Foufoula-Georgiou et al. 2015), and engineered structures in the floodplain (e.g., Munoz et al. 2018). Our results support the notion that valley morphology, a meso-scale physical constraint, plays a key role in modulating biophysical interactions across scales, ultimately impacting how inundation patterns are manifested in the river-floodplain valley and the development of valley landforms (Nanson and Croke 1992, Miller 1995, Jain et al. 2008, Fryirs and Brierley 2010, Thayer and Ashmore 2016, Cienciala and Pasternack 2017).

Wide river-valley settings can confer a high potential for flood pulse storage, particularly during moderate flows (Woltemade and Potter 1994, Turner-Gillespie et al. 2003), but peak flow attenuation can be comparatively lower during valley-filling stages as the volume of floodwater reaches depths to overcome floodplain frictional resistance (Turner-Gillespie et al. 2003). In our reaches, flooding resulted from interacting backwater effects, flow through internal drainage networks, and direct overbank wetting. We observed shorter times to peak for lower magnitude events in Seneca Creek and Patuxent River compared to higher magnitude events, and both study reaches were also characterized by frequent inundation, longer flood durations, and deeper surface water depths that would indicate high potentials for flood pulse storage.

Relatively confined river-valley settings have less capacity for attenuation of a flood wave, ceteris paribus (Woltemade and Potter 1994, Baker and Wiley 2009). Flooding dynamics at the confined Patapsco River and Little Gunpowder Falls reaches were largely due to direct wetting of topographic lows adjacent to the channel with little backwater filling. Reductions in the observed time to peak wetted extent in the Patapsco River and Little Gunpowder Falls reaches were consistent with other indicators of comparatively low storage capacity such as limited inundation extents, shorter average duration, and shallower depths. However, temporal evidence for flood-wave attenuation in these reaches was likely influenced by our decision to include point bars and topographic lows in the definition of out-of-channel flows. These areas were slow to drain and conveyed little water volume as a proportion of total flood volume; thus, their inclusion led to inflated recession period estimates in our temporal analysis.

The role of basin scale

Conceptual models of river systems that are based on continuously varying physical properties, such as the River Continuum Concept (RCC, Vannote et al. 1980), are inconsistent with our results. The RCC predicts proportionally greater material and nutrient subsidies from terrestrial areas in reaches with smaller contributing areas compared to larger contributing areas (Vannote et al. 1980), but our results demonstrate that large proportions of the valley-bottom surface can become hydrologically connected to the river channel in reaches with both large and small contributing areas. Instead, our results are consistent with hydrogeomorphic patch or functional

process zone perspectives in which geology, tributary junctions, and historical effects vary discontinuously throughout a basin (sensu Poole 2002, Benda et al. 2004, Thorp et al. 2006). Longitudinal patterns in the degree of lateral hydrologic connectivity can have implications for the functioning of both aquatic and floodplain ecosystems by influencing the downstream transfer of nutrients and organic materials, sediment storage dynamics, and sourcing and dispersal of organisms (Rice et al. 2001, Amoros and Bornette 2002, Bornette et al. 2008, Tabacchi et al. 2005, Fryirs et al. 2007, Ward 1998). Thus, it is important to recognize that basin scale alone may not necessarily be predictive of certain ecological patterns.

Although the relative distributions of flooding attributes were a function of river-valley morphology, the absolute values of duration, depth, and shear stress appeared more consistent across reaches of similar contributing areas rather than shape. In general, durations were shorter, depths were shallower, and shear stresses were more variable in valley bottoms from smaller basins. The maximum duration experienced on a valley bottom is limited by the overall duration of the event hydrograph, which is shorter in smaller vs. larger basins for similar rainfall events due to reduced flow storage, shorter times to flow concentration, and typically steeper channel slopes (Black 1997). Inundation depth is limited by the total volume of water available, which interacts with the surface topography of the valley bottom to determine the distribution of water depths during a flood event. In our simulations, smaller basins had lower peak discharges than in larger basins for any given quantile hydrograph (Appendix S1: Table S3), and as a result, less water was available to be distributed across the valley-bottom surface in smaller basins than in larger basins.

We observed a phase-shift change in the nature of flooding between the 50th and 75th quantile events for reaches with large contributing areas that was not observed in the reaches from smaller basins. Substantial changes in inundation extent, depth, and shear stress may be more related to the increase in peak flow discharges of the simulations than basin scale alone. Peak discharges during the 75th quantile event were 1.86 and 1.96 times greater than during the 50th quantile event for Seneca Creek and Patapsco River, respectively, while other increases between quantile events were almost always <1.25 (Appendix S1: Table S3). In contrast, changes in peak discharge between the 50th and 75th quantile events were smaller for the Patuxent River and Little Gunpowder Falls (128% and 151% increases, respectively), with greater shifts observed between the 25th and 50th quantile events (Appendix S1: Table S3). Additional simulations that have consistent increases in peak discharges across event magnitudes may be able to further isolate the relative role of basin size compared to event magnitude, but such an analysis was beyond the scope of this study.

The relationship between event magnitude and inundation dynamics

Patterns of within-reach flooding across event magnitudes revealed complex interactions between hydrology and surface topography that differentiated by valley type. In confined reaches, valley topography was relatively varied and over half of the valley surface remained dry during low-magnitude events (10th–50th quantile hydrographs). Distributions of inundation depth became more variable across the Patapsco floodplain surface during high-magnitude events (75th–90th quantile hydrographs) when stages were substantial enough to exceed bankfull stage along heavily incised channels. Duration was also highly variable at these reaches due to small proportions of the valley bottom becoming wetted and the presence of ponding near valley walls, particularly in the Little Gunpowder Falls reach. In contrast, valley surfaces in unconfined settings were relatively flatter and dissected with internal drainage networks that led to fundamentally different inundation dynamics. The dominant direction and nature of flooding in unconfined valleys shifted across flood event magnitudes: During low flows, inundation occurred primarily through backfilling and preferential routing through distributary drainage networks, and as discharge increased, the channel and floodplain acted as a single unit with flow in the down-valley direction to accommodate greater flood volumes. During recession, the internal drainage networks activated and routed flow off the floodplain surface, conveying water when discharges were less than bankfull flow. Our observation of the changing role of the internal drainage network is

consistent with the findings of Knight and Shiono (1996) who documented convergence in inundation depth and velocities across the floodplain and channel as flood magnitudes increased. However, the origins, evolution, and geomorphic and ecological functions of the internal drainage networks in our study reaches are underdescribed in the literature. Their prominence in our study reaches suggests that future work to describe their morphodynamics and ecohydrologic roles would contribute to a fuller understanding of unconfined, frequently inundated valleys in the Maryland Piedmont and elsewhere.

In addition to event magnitude, hydrograph shape can have a strong influence on peak flow attenuation (Woltemade and Potter 1994), a phenomenon observed in the Patuxent River reach. Low to intermediate magnitude events had shallower rising limbs, resulting in a low-energy flood wave that initiated valley-wide backfilling in the upper reach behind a road embankment; downstream of the embankment, inundation was not as extensive. Lateral connectivity in the downstream reach increased with event magnitude to result in shorter average durations with increasing quantile event. Only during the 90th quantile event did both upper and lower floodplain reaches experience similar durations.

Contribution of 2D hydraulic modeling to understanding floodplain ecosystems

Our results show that the manifestation of out-of-bank flows in valley floors can vary widely, even within a single physiographic province. Measures of frequency, duration, timing, and rate of change in streamflow records are used to characterize likely habitat conditions and disturbance regimes for aquatic endpoints (Poff 1996), to derive hydrologic classifications for ecological applications (Poff 1996, Harris et al. 2000, Monk et al. 2006, Kennard et al. 2010, Olden et al. 2012, McManamay et al. 2014), and to develop environmental flow standards for watershed management (Arthington et al. 2006, Kennen et al. 2009, Poff et al. 2010). Our results suggest that hydrologic and hydraulic conditions experienced on the valley floor surface during out-of-bank flow may not be well represented by existing hydrologic metrics derived from discharge data alone. Additional tools are therefore needed to describe spatially explicit inundation regimes within the broader hydrologic and geomorphic contexts and assess potential responses to management activities (Bond et al. 2014, Brewer et al. 2016, Kozak et al. 2016).

The ability to map inundation dynamics consistently within and among river reaches is a fundamental step in developing predictive relationships in floodplain ecosystems (Vaughan et al. 2009). Inundation has been measured in situ using instruments such as piezometers (e.g., Jacinthe et al. 2015, Rybicki et al. 2015), water level recorders (Kroes et al. 2015), and temperature sensors (Dietrich et al. 2015). Such methods provide precise characterizations of local inundation dynamics over relatively brief time spans, but are often labor-intensive and can limit biophysical inferences to the area and time span of data collection. In an attempt to generalize flooding dynamics to broader areas and longer time spans, hydrogeomorphic variables such as landform type (Osterkamp and Hupp 1984, Hupp and Osterkamp 1985), positioning within the river-valley bottom (Poole et al. 2002, Turner et al. 2004), and morphology of river reaches (Baker and Wiley 2009) have been used as surrogates for multiple hydro-physical attributes. Such variables are extractable from spatially continuous topographic datasets, but can mask interactive physical variables and may not translate well across multiple reaches or under different hydrologic regimes.

Our maps of recurrence interval are a novel application of unsteady 2D hydraulic modeling that addresses a long-standing need in floodplain ecology: a standardized way to characterize inundation patterns consistently both within and among reaches. In their seminal quantitative investigation into floodplain forest dynamics, Hupp and Osterkamp (1985) recognized the challenge of describing inundation dynamics consistently across floodplain landforms and suggested that assigning hydrologically defined flood frequencies to geomorphic features as an appropriate solution. Other studies have used steady hydraulic models to map a subset of design flow recurrence intervals across valley surfaces (e.g., Theiling and Burant 2013, Marks et al. 2014, Edwards et al. 2016), an approach also used in the development of flood hazard maps (NRC 2007). Inundation frequency has also been characterized by examining wetting and drying patterns resulting from

hydrodynamic modeling, with frequency summarized as occurrences of wetting events or as percentages of time inundated (Stone et al. 2017, Whipple 2018). Our maps of recurrence interval result from combining two important analytical tools: unsteady 2D hydraulic models, which are better suited to account for complex flow dynamics in river-valley settings represented in our study than 1D models (Horritt and Bates 2002), and standard flow frequency analysis, which is a fundamental tool for characterizing hydrology across sites (Interagency Committee on Water Data 1982). By linking the two approaches, we are able to extend the ideas of Hupp and Osterkamp (1985) to assign hydrologic measures of inundation at scales finer than the landforms themselves, which can be important for understanding how organisms interact with environmental conditions across a range of spatial resolutions. The resulting maps offer a standardized method of hydrologic comparison that is meaningful within and across study sites and, when combined with other summaries of flooding patterns (e.g., duration, depth, shear stress), allow for a comprehensive understanding of inundation regimes.

Maps of hydraulic model outputs such as flood depth, duration, and shear stress can provide other important descriptors of flooding dynamics that are comparable across reaches when the models have similar error levels (Wright et al. 2016) and can be useful for ecological investigations. Previous studies using 2D model output to characterize physical constraints on floodplain forests have successfully described linkages between river hydrology, lateral hydrologic connectivity, and forest composition (Meitzen 2011, Kupfer et al. 2015, Meitzen and Kupfer 2015) and predicted forest succession processes in response to physical gradients associated with flooding such as flooding depth, duration, and shear stress (Benjankar et al. 2012, Garciá-Arias et al. 2013, Rivaes et al. 2013, 2014). Recent applications of 2D hydraulic models have described how flooding regimes may shift in response to direct anthropogenic regulation of hydrology, climatic forcings, and their interactions (Karim et al. 2015, Whipple 2018), including changes in mass fluxes between the channel and floodplain (Stone et al. 2017).

Our models of unsteady flows revealed important differences in the role of backwater filling, internal drainage networks, and within-reach shifts in dominant flow direction through time. Flooding dynamics such as these may have important implications for biophysical interactions such as sediment dynamics, primary production, and organic matter transport (Irion et al. 1997, Galat et al. 1998, Sparks et al. 1998, Tockner et al. 2000). Without the use of unsteady hydraulic models, however, such dynamics would be difficult to characterize or quantify.

At the same time, hydraulic models, including the 2D HEC-RAS model employed in this study, may have limitations in ecological applications. In particular, without coupling to models of groundwater or precipitation, HEC-RAS is limited to modeling surface flow; other mechanisms of inundation such as groundwater inputs, overtopping of tributaries adjacent to the floodplain, direct rainfall or hillslope contributions (Mertes 1997) are not explicitly captured. Thus, hydraulic models that account for only surface water dynamics may predict a more limited range of inundation dynamics for reaches like Seneca Creek, where we observed evidence of groundwater seeps near the hillslope and flow in secondary channels throughout the year. The distinction between Seneca Creek and the Patapsco River is likely to be even greater due to underestimates of inundation frequency. At the Patuxent River, the distribution of fresh, coarse-grained sedimentary deposits following storm events suggests that flows from intermittent lateral tributaries onto the valley floor may also contribute to inundation dynamics. The model as applied here was not intended to capture these processes. Additional data or analyses may be needed to bolster output from hydraulic models when linking to ecological data. Nonetheless, spatially explicit hydraulic models offer a promising approach to documenting spatial patterns and processes of flooding for ecological purposes (Meitzen et al. 2013). Our results, along with previous studies that have used similar models to describe inundation dynamics for ecological purposes, indicate that there is great potential for 2D hydraulic models to advance process-based knowledge of floodplain ecosystems.

Acknowledgments

The authors are grateful for fieldwork assistance by Meghna Bhatt, Briana Diacopoulos, Grzegorz Gurda,

Tabrina Hughes, Nicati Robideaux, and David and Linda Van Appledorn. Mariya Shcheglovitova provided scripting assistance. Two anonymous reviewers and Jennifer Sauer provided insightful critiques that improved the manuscript. Molly Van Appledorn completed this work at the Department of Geography and Environmental Systems, University of Maryland Baltimore County, prior to employment with the U.S. Geological Survey with support from Maryland Sea Grant awards NA10OAR4170072 and NA14OAR4170090 from the National Oceanic and Atmospheric Administration, U.S. Department of Commerce. The authors declare no conflict of interest. Use of trade, product, or firm names does not imply endorsement by the U.S. Government.

Literature Cited

Amoros, C., and G. Bornette. 2002. Connectivity and biocomplexity in waterbodies of riverine floodplains. Freshwater Biology 47:761–776.

Arthington, A. H., S. E. Bunn, N. L. Poff, and R. J. Naiman. 2006. The challenge of providing environmental flow rules to sustain river ecosystems. Ecological Applications 16:1311–1318.

Baker, M. E., and M. J. Wiley. 2009. Multiscale control of flooding and riparian-forest composition in Lower Michigan, USA. Ecology 90:145–159.

Benda, L. E. E., N. L. Poff, D. Miller, T. Dunne, G. Reeves, G. Pess, and M. Pollock. 2004. The network dynamics hypothesis: How channel networks structure riverine habitats. BioScience 54:413–427.

Bendix, J., and C. R. Hupp. 2000. Hydrological and geomorphological impacts on riparian plant communities. Hydrological Processes 14:2977–2990.

Benjankar, R., K. Jorde, E. M. Yager, G. Egger, P. Goodwin, and N. F. Glenn. 2012. The impact of river modification and dam operation on floodplain vegetation succession trends in the Kootenai River, USA. Ecological Engineering 46:88–97.

Bernhardt, E. S., et al. 2005. Synthesizing U.S. river restoration efforts. Science 308:636–637.

Black, P. E. 1997. Watershed functions. Journal of the American Water Resources Association 33:1–11.

Bond, N., J. Costelloe, A. King, D. Warfe, P. Reich, and S. Balcombe. 2014. Ecological risks and opportunities from engineered artificial flooding as a means of achieving environmental flow objectives. Frontiers in Ecology and the Environment 12:386–394.

Bornette, G., E. Tabacchi, C. Hupp, S. Puijalon, and J. C. Rostan. 2008. A model of plant strategies in fluvial hydrosystems. Freshwater Biology 53:1692–1705.

Bravard, J. P., C. Amoros, G. C. Pautou, G. Bornette, M. Bournaud, M. Creuzé des Châtelliers, J. Gilbert, J. L. Peiry, J. F. Perrin, and H. Tachet. 1997. Stream incision in Southeast France: morphological phenomena and impacts upon biocenoses. Regulated Rivers 13:75–90.

Brewer, S. K., R. A. McManamay, A. D. Miller, R. Mollenhauer, T. A. Worthington, and T. Arsuffi. 2016. Advancing environmental flow science: developing frameworks for altered landscapes and integrating efforts across disciplines. Environmental Management 58:175–192.

Brierley, G. J., and K. Fryirs. 2005. Geomorphology and river management: applications of the river styles framework. Blackwell, Oxford, UK.

Chow, V. T. 1959. Open channel hydraulics. McGraw-Hill, New York, New York, USA.

Cienciala, P., and G. B. Pasternack. 2017. Floodplain inundation response to climate, valley form, and flow regulation on a gravel-bed river in a Mediterranean-climate region. Geomorphology 282:1–17.

Corenblit, D., A. C. Baas, G. Bornette, J. Darrozes, S. Delmotte, R. A. Francis, A. M. Gurnell, F. Julien, R. J. Naiman, and J. Steiger. 2011. Feedbacks between geomorphology and biota controlling Earth surface processes and landforms: a review of foundation concepts and current understandings. Earth-Science Reviews 106:307–331.

Davies-Colley, R. J. 1997. Stream channels are narrower in pasture than in forest. New Zealand Journal of Marine and Freshwater Research Abstracts 31:599–608.

Dietrich, A. L., C. Nilsson, and R. Jansson. 2015. A phytometer study evaluating the effects of stream restoration on riparian vegetation. Ecohydrology 9:646–658.

Donovan, M., A. Miller, M. Baker, and A. Gellis. 2015. Sediment contributions from floodplains and legacy sediments to Piedmont Streams of Baltimore County, Maryland. Geomorphology 235:88–105.

Edwards, B. L., R. F. Keim, E. L. Johnson, C. R. Hupp, S. Marre, and S. L. King. 2016. Geomorphic adjustment to hydrologic modifications along a meandering river: implications for surface flooding on a floodplain. Geomorphology 269:149–159.

Foufoula-Georgiou, E., Z. Takbiri, J. A. Czuba, and J. Schwenk. 2015. The change of nature and the nature of change in agricultural landscapes: Hydrologic regime shifts modulate ecological transitions. Water Resources Research 51:6649–6671.

Frye, R. J., and J. A. Quinn. 1979. Forest development in relation to topography and soils on a floodplain of the Raritan River, New Jersey. Bulletin of the Torrey Botanical Club 106:334–335.

Fryirs, K. A., and G. J. Brierley. 2010. Antecedent controls on river character and behavior in partly confined valley settings: upper Hunter catchment, NSW, Australia. Geomorphology 117:106–120.

Fryirs, K. A., and G. J. Brierley. 2013. Geomorphic analysis of river systems: an approach to reading the landscape. John Wiley & Sons, Chichester, UK.

Fryirs, K. A., G. J. Brierley, N. J. Preston, and J. Spencer. 2007. Catchment scale (dis)connectivity in sediment flux in the upper Hunter catchment, New South Wales, Australia. Geomorphology 84:297–316.

Fryirs, K. A., J. M. Wheaton, and G. J. Brierley. 2016. An approach for measuring confinement and assessing the influence of valley setting on river forms and processes. Earth Surface Processes and Landforms 41:701–710.

Galat, D. L., et al. 1998. Flooding to restore connectivity of regulated, large-river wetlands. BioScience 48:721–733.

García-Arias, A., F. Francés, T. Ferreira, G. Egger, F. Martínez-Capel, V. Garófano-Gómez, I. Andrés-Doménech, E. Politti, R. Rivaes, and P. M. Rodríguez-González. 2013. Implementing a dynamic riparian vegetation model in three European river systems. Ecohydrology 6:635–651.

Gregory, K. J. 1992. Vegetation and river channel processes. Pages 255–269 *in* P. J. Boon, P. Calow, and G. E. Petts, editors. River conservation and management. Wiley, Chichester, UK.

Gregory, S. V., F. J. Swanson, W. A. McKee, and K. W. Cummins. 1991. An ecosystem perspective of riparian zones. BioScience 41:540–551.

Gurnell, A. M., and G. E. Petts. 2003. Island dominated landscapes of large floodplain rivers: a European perspective. Freshwater Biology 47:581–600.

Harris, N. M., A. M. Gurnell, D. M. Hannah, and G. E. Petts. 2000. Classification of river regimes: a context for hydroecology. Hydrological Processes 14:2831–2848.

Horritt, M. S., and P. D. Bates. 2002. Evaluation of 1D and 2D numerical models for predicting river flood inundation. Journal of Hydrology 268:87–99.

Hughes, F. M. R. 1997. Floodplain biogeomorphology. Progress in Physical Geography 21:501–529.

Hupp, C. R. 2000. Hydrology, geomorphology and vegetation of coastal plain rivers in the south-eastern USA. Hydrological Processes 14:2991–3010.

Hupp, C. R., and D. E. Bazemore. 1993. Temporal and spatial patterns of wetland sedimentation, West Tennessee. Journal of Hydrology 141:179–196.

Hupp, C. R., and W. R. Osterkamp. 1985. Bottomland vegetation distribution along Passage Creek, Virginia, in relation to fluvial landforms. Ecology 66:670–681.

Interagency Advisory Committee on Water Data. 1982. Guidelines for determining flood-flow frequency. Bulletin 17B. Hydrology Subcommittee, Office of Water Data Coordination, U.S. Geological Survey, Reston, Virginia, USA. http://water.usgs.gov/osw/bulletin17b/bulletin_17B.html

Irion, G., W. J. Junk, and J. A. S. N. de Mello. 1997. The large central Amazonian river floodplains near Manaus: geological, climatological, hydrological and geomorphological aspects. Pages 23–46 *in* W. J. Junk, editor. The Central Amazon floodplain. Springer-Verlag, New York, New York, USA.

Jacinthe, P. A., P. Vidon, K. Fisher, X. Liu, and M. E. Baker. 2015. Soil methane and carbon dioxide fluxes from cropland and riparian buffers in different hydrogeomorphic settings. Journal of Environment Quality 44:1080–1090.

Jacobson, R. B., and D. J. Coleman. 1986. Stratigraphy and recent evolution of Maryland Piedmont Flood Plains. American Journal of Science 286:617–637.

Jain, V., K. Fryirs, and G. Brierley. 2008. Where do floodplains begin? The role of total stream power and longitudinal profile form on floodplain initiation processes. GSA Bulletin 120:127–141.

Johnson, W. C., R. L. Burgess, and W. R. Keammerer. 1976. Forest overstory vegetation and environment on the Missouri River floodplain in North Dakota. Ecological Monographs 46:59–84.

Jowett, I. G., and M. J. Duncan. 2012. Effectiveness of 1D and 2D hydraulic models for instream habitat analysis in a braided river. Ecological Engineering 48:92–100.

Junk, W. J., P. B. Bayley, and R. E. Sparks. 1989. The flood pulse concept in river-floodplain systems. Canadian Special Publication of Fisheries and Aquatic Sciences 106:110–127.

Kaase, C. T., and J. A. Kupfer. 2016. Sedimentation patterns across a Coastal Plain floodplain: the importance of hydrogeomorphic influences and cross-floodplain connectivity. Geomorphology 269:43–55.

Karim, F., D. dutta, S. Marvanek, C. Petheram, C. Ticehurst, J. Lerat, S. Kim, and A. Yang. 2015. Assessing the impacts of climate change and dams on floodplain inundation and wetland connectivity in the wet-dry tropics of northern Australia. Journal of Hydrology 522:80–94.

Kennard, M. J., B. J. Pusey, J. D. Olden, S. J. Mackay, J. L. Stein, and N. Marsh. 2010. Classification of natural flow regimes in Australia to support environmental flow management. Freshwater Biology 55:171–193.

Kennen, J. G., J. A. Henriksen, J. Heasley, B. S. Cade, and J. W. Terrell. 2009. Application of the hydroecological integrity assessment process for Missouri streams. Open-File Report 2009-1138. U.S. Geological Survey, Reston, Virginia, USA.

Knight, D. W., and K. Shiono. 1996. River channel and floodplain hydraulics. Pages 139–181 *in* M. Anderson, P. Bates, and D. Walling, editors. Floodplain processes. John Wiley and Sons, New York, New York, USA.

Kozak, J. P., M. G. Bennett, B. P. Piazza, and J. W. F. Remo. 2016. Towards dynamic flow regime management for floodplain restoration in the Atchafalaya River Basin, Louisiana. Environmental Science and Policy 64:118–128.

Kroes, D. E., E. R. Schenk, G. B. Noe, and A. J. Benthem. 2015. Sediment and nutrient trapping as a result of a temporary Mississippi River floodplain restoration: the Morganza Spillway during the 2011 Mississippi River Flood. Ecological Engineering 82:91–102.

Kupfer, J. A., K. M. Meitzen, and P. Gao. 2015. Flooding and surface connectivity of *Taxodium-Nyssa* stands in a southern floodplain forest ecosystem. River Research and Applications 31:1299–1310.

Leopold, L. B. 1994. A view of the river. Harvard University Press, Boston, Massachusetts, USA.

Leopold, L. B., and T. Maddock Jr. 1953. The hydraulic geometry of stream channels and some physiographic implications. U.S. Geological Survey, Washington, D.C., USA.

Lóczy, D., E. Pirkhoffer, and P. Gyenizse. 2012. Geomorphometric floodplain classification in a hill region of Hungary. Geomorphology 147–148:61–72.

Malanson, G. P. 1993. Riparian landscapes. Cambridge University Press, Cambridge, UK.

Marks, C. O., K. H. Nislow, and F. J. Magilligan. 2014. Quantifying flooding regime in floodplain forests to guide river restoration. Elementa: Science of the Anthropocene 2:000031.

Marston, R. A., J. Girel, G. C. Pautou, H. Piégay, J.-P. Bravard, and C. Arneson. 1995. Channel metamorphosis, floodplain disturbance, and vegetation development, Ain River, France. Geomorphology 13:121–131.

Maryland Geological Survey. 1968. Geologic map of Maryland. http://www.mgs.md.gov/esic/geo/index.html

McManamay, R. A., M. S. Bevelhimer, and S.-C. Kao. 2014. Updating the US hydrologic classification: an approach to clustering and stratifying ecohydrologic data. Ecohydrology 7:903–926.

Megonigal, J. P., W. H. Conner, S. Kroeger, and R. R. Sharitz. 1997. Aboveground production in southeastern floodplain forests: a test of the subsidy-stress hypothesis. Ecology 78:370–384.

Meitzen, K. M. 2011. Flood processes, forest dynamics, and disturbance in the Congaree River floodplain, South Carolina. Dissertation. University of South Carolina, Columbia, South Carolina, USA. https://scholarcommons.sc.edu/etd/1296

Meitzen, K. M., M. W. Doyle, M. C. Thoms, and C. E. Burns. 2013. Geomorphology within the interdisciplinary science of environmental flows. Geomorphology 200:143–154.

Meitzen, K. M., and J. A. Kupfer. 2015. Abandoned meander forest development patterns in a large alluvial southeastern floodplain, South Carolina, USA. River Systems 21:141–162.

Merritts, D., et al. 2011. Anthropocene streams and base-level controls from historic dams in the unglaciated mid-Atlantic region, USA. Philosophical Transactions of the Royal Society A 369:976–1009.

Mertes, L. A. 1997. Documentation and significance of the perirheic zone on inundated floodplains. Water Resources Research 33:1749–1762.

Miller, A. J. 1995. Valley morphology and boundary conditions influencing spatial patterns of flood flow. Pages 57–81 *in* J. E. Costa, A. J. Miller, K. W. Potter, and P. R. Wilcock, editors. Natural and anthropogenic influences in fluvial geomorphology. American Geophysical Union, Washington, D.C., USA.

Monk, W. A., P. J. Wood, D. M. Hannah, D. A. Wilson, C. A. Extence, and R. P. Chadd. 2006. Flow variability and macroinvertebrate community response within riverine systems. River Research and Applications 22:595–615.

Munoz, S. E., L. Giosan, M. D. Therrell, J. W. F. Remo, Z. Shen, R. M. Sullivan, C. Wiman, M. O'Donnell, and J. P. Donnelly. 2018. Climatic control of Mississippi River flood hazard amplified by river engineering. Nature 556:95–98.

Naiman, R. J., and H. Decamps. 1997. The ecology of interfaces: riparian zones. Annual Review of Ecology and Systematics 28:621–658.

Naiman, R. J., H. Décamps, and M. Pollock. 1993. The role of riparian corridors in maintaining regional diversity. Ecological Applications 3:209–212.

Nakamura, F., and N. Shin. 2001. The downstream effects of dams on the regeneration of riparian tree species in northern Japan. Pages 173–181 *in* J. M. Dorava, D. R. Montgomery, B. B. Palcsak, and F. A. Fitzpatrick, editors. Geomorphic processes and riverine habitat. Water Science Application series. Volume 4. American Geophysical Union, Washington, D.C., USA.

Nakamura, F., N. Shin, and S. Inahara. 2007. Shifting mosaic in maintaining diversity of floodplain tree species in the northern temperate zone of Japan. Forest Ecology and Management 241:28–38.

Nanson, G. C., and J. C. Croke. 1992. A genetic classification of floodplains. Geomorphology 4:459–486.

National Research Council. 2007. Elevation data for floodplain mapping. Committee on Floodplain Mapping Technologies. National Academy Press, Washington, D.C., USA.

Noe, G. B., and C. R. Hupp. 2009. Retention of riverine sediment and nutrient loads by coastal plain floodplains. Ecosystems 12:728–746.

Olde Venterink, H., J. E. Vermaat, M. Pronk, F. Wiegman, G. E. M. van der Lee, M. W. van den Hoorn, L. W. G. Higler, and J. T. A. Verhoeven. 2006. Importance of sediment deposition and denitrification for nutrient retention in floodplain wetlands. Applied Vegetation Science 9:163–174.

Olden, J. D., M. J. Kennard, and B. J. Pusey. 2012. A framework for hydrologic classification with a review of methodologies and applications in ecohydrology. Ecohydrology 5:503–518.

Osterkamp, W. R., and C. R. Hupp. 1984. Geomorphic and vegetative characteristics along three northern Virginia streams. Bulletin of the Geological Society of America 95:1093–1101.

Pautou, G. C., and M.-F. Arens. 1994. Theoretical habitat templates, species traits, and species richness: floodplain vegetation in the Upper Rhône River. Freshwater Biology 31:507–522.

Poff, N. L. 1996. A hydrogeography of unregulated streams in the United States and an examination of scale-dependence in some hydrological descriptors. Freshwater Biology 36:71–91.

Poff, N. L., et al. 2010. The ecological limits of hydrologic alteration (ELOHA): a new framework for developing regional environmental flow standards: Ecological limits of hydrologic alteration. Freshwater Biology 55:147–170.

Poole, G. C. 2002. Fluvial landscape ecology: addressing uniqueness within the river discontinuum. Freshwater Biology 47:641–660.

Poole, G. C., J. A. Stanford, C. A. Frissell, and S. W. Running. 2002. Three-dimensional mapping of geomorphic controls on flood-plain hydrology and connectivity from aerial photos. Geomorphology 48:329–347.

R Development Core Team. 2016. R: a language and environment for statistical computing. R Foundation for Statistical Computing, Vienna, Austria.

Rice, S. P., M. T. Greenwood, and C. B. Joyce. 2001. Tributaries, sediment sources, and the longitudinal organisation of macroinvertebrate fauna along river systems. Canadian Journal of Fisheries and Aquatic Sciences 58:824–840.

Ries, K. G., III, M. A. Horn, M. R. Nardi, and S. Tessler. 2010. Incorporation of water-use summaries into the StreamStats web application for Maryland. U.S. Geological Survey Scientific Investigations Report 2010–5111, 18p.

Rinaldi, M., N. Surian, F. Comiti, and M. Bussettini. 2013. A method for the assessment and analysis of the hydromorphological condition of Italian streams: the Morphological Quality Index (MQI). Geomorphology 180–181:96–108.

Rivaes, R., P. M. Rodríguez-González, A. Albuquerque, A. N. Pinheiro, G. Egger, and M. T. Ferreira. 2013. Riparian vegetation responses to altered flow regimes driven by climate change in Mediterranean rivers. Ecohydrology 6:413–424.

Rivaes, R. P., P. M. Rodriguez-Gonzalez, M. T. Ferreira, A. N. Pinheiro, E. Politti, G. Egger, A. García-Arias, and F. Frances. 2014. Modeling the evolution of riparian woodlands facing climate change in three European rivers with contrasting flow regimes. PLoS ONE 9:e110200.

Rybicki, N. B., G. B. Noe, C. Hupp, and M. E. Robinson. 2015. Vegetation composition, nutrient, and sediment dynamics along a floodplain landscape. River Systems 21:109–123.

Scown, M. W., M. C. Thoms, and N. R. De Jager. 2015. Floodplain complexity and surface metrics: influences of scale and geomorphology. Geomorphology 245:102–116.

Sparks, R. E., J. C. Nelson, and Y. Yin. 1998. Naturalization of the flood regime in regulated rivers. BioScience 48:706–720.

Sparks, R. E., and A. Spink. 1998. Disturbance, succession and ecosystem processes in rivers and estuaries: effects of extreme hydrologic events. Regulated Rivers: Research & Management 14:155–159.

Stone, M. C., C. F. Byrne, and R. R. Morrison. 2017. Evaluating the impacts of hydrologic and geomorphic alterations on floodplain connectivity. Ecohydrology 10:e1833.

Tabacchi, E., R. Correll, G. Pinay, A.-M. Planty-Tabacchi, and R. C. Wissmar. 1998. Development, maintenance, and the role of riparian vegetation in the river landscape. Freshwater Biology 40:497–516.

Tabacchi, E., A.-M. Planty-Tabacchi, and O. Décamps. 1990. Continuity and discontinuity of the riparian vegetation along a fluvial corridor. Landscape Ecology 5:9–20.

Tabacchi, E., A.-M. Planty-Tabacchi, L. Roques, and E. Nadal. 2005. Seed inputs in riparian zones: implications for plant invasion. River Research and Applications 21:299–313.

Thayer, J. B., and P. Ashmore. 2016. Floodplain morphology, sedimentology, and development processes of a partially alluvial channel. Geomorphology 269:160–174.

Theiling, C. H., and J. T. Burant. 2013. Flood inundation mapping for integrated floodplain management. River Research and Applications 29: 961–978.

Thomas, W. O., Jr, and G. E. Moglen. 2010. An update of regional regression equations for Maryland. Appendix 3. Pages 135–172 *in* Application of Hydrologic Methods in Maryland. Third edition. Maryland State Highway Administration and Maryland Department of the Environment, Annapolis, Maryland.

Thorp, J. H., M. C. Thoms, and M. D. Delong. 2006. The riverine ecosystem synthesis: biocomplexity in river networks across space and time. River Research and Applications 22:123–147.

Tockner, K., F. Malard, and J. V. Ward. 2000. An extension of the flood pulse concept. Hydrological Processes 14:2861–2883.

Tockner, K., and J. A. Stanford. 2002. Riverine flood plains: present state and future trends. Environmental Conservation 29:308–330.

Turner, M. G., S. E. Gergel, M. D. Dixon, and J. R. Miller. 2004. Distribution and abundance of trees in floodplain forests of the Wisconsin River: environmental influences at different scales. Journal of Vegetation Science 15:729–738.

Turner-Gillespie, D. F., J. A. Smith, and P. D. Bates. 2003. Attenuating reaches and the regional flood response of an urbanizing drainage basin. Advances in Water Resources 26:673–684.

USGS. 2007. User's manual for Program PeakFQ, annual flood-frequency analysis using Bulletin 17B Guidelines. U.S. Geological Survey, Washington, D.C., USA.

Van Appledorn, M. 2016. Evaluating the nature and strength of environmental control on floodplain forest communities. Dissertation. University of Maryland Baltimore County, Baltimore, Maryland, USA.

Vannote, R. L., G. W. Minshall, K. W. Cummins, J. R. Sedell, and C. E. Cushing. 1980. The river continuum concept. Canadian Journal of Fisheries and Aquatic Sciences 37:130–137.

Vaughan, I. P., M. Diamond, A. M. Gurnell, K. A. Hall, A. Jenkins, N. J. Milner, L. A. Naylor, D. A. Sear, G. Woodward, and S. J. Ormerod. 2009. Integrating ecology with hydromorphology: a priority for river science and management. Aquatic Conservation: Marine and Freshwater Ecosystems 19:113–125.

Viles, H. 2016. Technology and geomorphology: Are improvements in data collection techniques transforming geomorphic science? Geomorphology 270:121–133.

Walter, R. C., and D. J. Merritts. 2008. Natural streams and the legacy of water-powered mills. Science 319:299–304.

Ward, J. V. 1998. Riverine landscapes: biodiversity patterns, disturbance regimes, and aquatic conservation. Biological Conservation 83:269–278.

Ward, J. V., K. Tockner, D. B. Arscott, and C. Claret. 2002. Riverine landscape diversity. Freshwater Biology 47:517–539.

Whipple, A. A. 2018. Managing flow regimes and landscapes together: hydrospatial analysis for evaluating spatiotemporal floodplain inundation patterns with restoration and climate change implications. Dissertation. University of California Davis, Davis, California, USA.

White, K. E. 2001. Regional curve development and selection of a reference reach in the non-urban, lowland sections of the Piedmont Physiographic Province, Pennsylvania and Maryland. Water Resources Investigations Report. U.S. Geological Survey, Washington, D.C., USA.

Wolman, B. M., and L. B. Leopold. 1957. River flood plains: some observations on their formation. Professional Paper 282C: 87–107. U.S. Geological Survey, Washington, D.C., USA.

Woltemade, C. J. 1994. Form and process: fluvial geomorphology and flood-flow interaction, Grant River, Wisconsin. Annals of the Association of American Geographers 84:462–479.

Woltemade, C. J., and K. W. Potter. 1994. A watershed modeling analysis of fluvial geomorphologic influences on flood peak attenuation. Water Resources Research 30:1933–1942.

Wright, K. A., D. H. Goodman, N. A. Som, J. Alvarez, A. Martin, and T. B. Hardy. 2016. Improving hydrodynamic modelling: an analytical framework for assessment of two-dimensional hydrodynamic models. River Research and Applications 33:170–181.

Data Availability

Data associated with this paper are available at: https://doi.org/10.5066/p9itqtnq.

Supporting Information

Additional Supporting Information may be found online at: http://onlinelibrary.wiley.com/doi/10.1002/ecs2.2546/full